Journal of Virology

Cryo-Electron Microscopy Structure of Adenovirus Type 2 Temperature-Sensitive Mutant 1 Reveals Insight into the Cell Entry Defect

Mariena Silvestry, Steffen Lindert, Jason G. Smith, Oana Maier, Christopher M. Wiethoff, Glen R. Nemerow and Phoebe L. Stewart

***J. Virol.* 2009, 83(15):7375. DOI: 10.1128/JVI.00331-09.**
Published Ahead of Print 20 May 2009.

JOURNAL OF VIROLOGY, Aug. 2009, p. 7375–7383 Vol. 83, No. 15
0022-538X/09/$08.00+0 doi:10.1128/JVI.00331-09

Cryo-Electron Microscopy Structure of Adenovirus Type 2 Temperature-Sensitive Mutant 1 Reveals Insight into the Cell Entry Defect▽†

Mariena Silvestry,[1] Steffen Lindert,[1,2] Jason G. Smith,[3] Oana Maier,[4] Christopher M. Wiethoff,[4] Glen R. Nemerow,[3] and Phoebe L. Stewart[1]*

Department of Molecular Physiology and Biophysics, Vanderbilt University Medical Center, 2215 Garland Avenue, Nashville, Tennessee 37232[1]; Department of Chemistry, Vanderbilt University, Nashville, Tennessee 37212[2]; Department of Immunology and Microbial Science, The Scripps Research Institute, 10550 North Torrey Pines Road, IMM-19, La Jolla, California 92037[3]; and Department of Microbiology and Immunology, Loyola University Chicago Stritch School of Medicine, Loyola University Chicago, Building 105, 2160 South First Avenue, Maywood, Illinois 60153[4]

Received 13 February 2009/Accepted 11 May 2009

The structure of the adenovirus type 2 temperature-sensitive mutant 1 (Ad2*ts*1) was determined to a resolution of 10 Å by cryo-electron microscopy single-particle reconstruction. Ad2*ts*1 was prepared at a nonpermissive temperature and contains the precursor forms of the capsid proteins IIIa, VI, and VIII; the core proteins VII, X (mu), and terminal protein (TP); and the L1-52K protein. Cell entry studies have shown that although Ad2*ts*1 can bind the coxsackievirus and Ad receptor and undergo internalization via αv integrins, this mutant does not escape from the early endosome and is targeted for degradation. Comparison of the Ad2*ts*1 structure to that of mature Ad indicates that Ad2*ts*1 has a different core architecture. The Ad2*ts*1 core is closely associated with the icosahedral capsid, a connection which may be mediated by preproteins IIIa and VI. Density within hexon cavities is assigned to preprotein VI, and membrane disruption assays show that hexon shields the lytic activity of both the mature and precursor forms of protein VI. The internal surface of the penton base in Ad2*ts*1 appears to be anchored to the core by interactions with preprotein IIIa. Our structural analyses suggest that these connections to the core inhibit the release of the vertex proteins and lead to the cell entry defect of Ad2*ts*1.

Cryo-electron microscopy (cryo-EM) studies of adenovirus (Ad) combined with atomic resolution structures of component proteins (hexon, penton base, fiber, and protease) have led to a detailed structural model for the mature Ad virion (31). While the Ad protein capsid is icosahedral, the core does not follow the overall symmetry of the particle, and thus the core is not well represented in cryo-EM structures (43). The core is composed of the 36-kb double-stranded DNA (dsDNA) genome complexed with four viral proteins (V, VII, mu, and terminal protein [TP]) and the virally encoded cysteine protease. The core of the mature virion may also contain a few copies of the L1-52K protein (7), a possible scaffolding protein that is present in higher copy numbers in assembling virions (18).

The capsid contains the major capsid proteins, hexon, penton base, and fiber, together with four minor capsid proteins (IIIa, VI, VIII, and IX). Cryo-EM difference mapping analyses have led to revised assignments for the locations of the minor capsid proteins, with protein IX on the exterior and the other three proteins on the inner capsid surface (9, 38). A scanning transmission EM study indicated that four trimers of protein IX stabilize the group of nine hexons in the center of each facet (11). However, more recent cryo-EM studies indicated that only the N-terminal domain of protein IX forms these trimeric assemblies (37, 38), while the C-terminal domain, which has a long predicted α-helix with strong propensity for coiled coil formation, associates in helical bundles at the facet edges (38). Two cryo-EM studies support the assignment of the tetrameric helical bundle on the capsid exterior to the C-terminal domain of protein IX (10, 23). Curiously, 12 monomers of protein IX per facet assemble into four trimers with their N-terminal domains and three tetramers with their C-terminal domains.

The internal location for protein IIIa below the penton base and surrounding peripentonal hexons was confirmed by a study of virions with N-terminally tagged protein IIIa (39). Although the locations for proteins VI and VIII have not been experimentally confirmed, these proteins are more than likely on the internal side of the capsid, as there is no remaining unassigned cryo-EM density on the exterior of the capsid. In addition, proteins VI and VIII are two of the viral proteins that are produced in precursor form and cleaved by the viral protease during maturation of the assembled virion (22). The protease is presumed to be packaged within the interior of the virion, and therefore the assignment of proteins VI and VIII to the interior of the capsid where they would be accessible to the protease is logical. Density within the internal cavity of all 240 hexon trimers in the Ad capsid has been assigned to protein VI on the basis of biochemical and temperature sensitivity studies (38, 51).

Ad cell entry begins with attachment of the Ad fiber to either

* Corresponding author. Mailing address: Vanderbilt University Medical Center, Department of Molecular Physiology and Biophysics, 710 Light Hall, 2215 Garland Avenue, Nashville, TN 37232. Phone: (615) 322-7908. Fax: (615) 322-7236. E-mail: phoebe.stewart@vanderbilt.edu.

† Supplemental material for this article may be found at http://jvi.asm.org/.

▽ Published ahead of print on 20 May 2009.

coxsackievirus and Ad receptor (3) or CD46 (12), which serve as the primary attachment receptors for Ad on most cell types (31). Internalization via clathrin-mediated endocytosis is triggered by association of the Ad penton base with αv integrins (49). Escape from the endosome is facilitated by the membrane lytic activity of protein VI, which is released from the virion in the low-pH environment of the early endosome (50). The stepwise dismantling of the Ad virion during cell entry has been described biochemically (15) but has not been fully characterized structurally. After endosomal escape, the partially uncoated Ad virion is transported along microtubules (44) to the nucleus, where the viral genome is inserted into the nucleus via a nuclear pore complex.

Propagation of an Ad2 temperature-sensitive mutant (Ad2*ts*1) at nonpermissive temperatures (>39°C) results in the synthesis of virions that have an uncoating defect (28, 30, 46). Although these Ad2*ts*1 particles are capable of interacting with coxsackievirus and Ad receptor and undergoing internalization via association with αv integrins, they are unable to escape the early endosome and thus are targeted for degradation in lysosomes (13, 14). The Ad2*ts*1 genetic defect is a point mutation (P137L) in protease that is linked to a defect in packaging into the virion (33). In wild-type Ad virions, the protease is activated inside nascent virions by the viral DNA as well as an 11-amino-acid peptide from the C-terminal end of protein VI (22). The Ad protease mediates the maturational cleavage of six structural proteins, i.e., IIIa, VI, VII, VIII, mu, and TP, as well as the presumed scaffolding protein L1-52K (26, 47, 48). In Ad2*ts*1 particles these cleavages do not occur. The presence of the precursor forms of these proteins in Ad2*ts*1 is associated with greater capsid stability (42, 50).

Here we present a cryo-EM structural study of the Ad2*ts*1 particle that provides insight into the cell entry defect of this temperature-sensitive mutant. Comparison of the Ad2*ts*1 structure with that of a mature Ad virion indicates that the major differences are in the interior of the virion.

MATERIALS AND METHODS

Preparation and isolation of Ad2*ts*1. A549 cells were maintained in Dulbecco's complete modified Eagle's medium supplemented with 10 mM HEPES, 2 mM L-glutamine, 1 mM sodium pyruvate, 0.1 mM nonessential amino acids, 100 U of penicillin G/ml, 0.3 mg of gentamicin/ml, and 10% fetal bovine serum. The temperature-sensitive mutant Ad2*ts1* was propagated in A459 cells at the nonpermissive temperature of 39.5°C. Cells were infected at a multiplicity of infection of 300 particles/cell with Ad2*ts1* that had been previously grown at the permissive temperature of 33°C. Infected cells were harvested after nearly complete cytopathic effect, approximately 60 h postinfection. Virus was purified from freeze/thaw lysates by two rounds of CsCl density gradient ultracentrifugation, dialyzed against Tris buffer at pH 8.0 (50 mM Tris, 130 mM NaCl, and 3 mM KCl), and immediately prepared for cryo-EM. Ad2*ts*1 particles were compared to wild-type Ad5 particles for the presence of unprocessed (preprotein) capsid proteins as determined by sodium dodecyl sulfate-polyacrylamide gel electrophoresis.

Cryo-EM. Cryo-EM grids were prepared as described by Saban et al. (37). Briefly, 6-μl samples of Ad2*ts*1 at a concentration of 614 μg/ml were applied to Quantifoil R2/4 holey carbon grids (Quantifoil Micro Tools GmbH) and vitrified using the Vitrobot cryofixation device (FEI Company). Data collection was performed on an FEI Polara (300 kV; FEG) transmission cryo-EM operated at liquid nitrogen temperature and 300 kV with a Gatan UltraScan 4kx4k charge-coupled device camera. Eight data sets were collected with a total of 7,218 cryo-EMs. Data sets 1 through 4 were collected manually, and data sets 5 through 8 were collected using SAM, a semiautomatic data collection routine (40). The absolute magnification for all data sets was ~×398,000.

Image processing. A total of 5,544 particle images were selected from the micrographs using the automatic selection program VIRUS (1). The particles were binned to 250^2 pixels (4.6-Å pixels) for the initial rounds of refinement, and later to 500^2 or 750^2 for processing with finer pixel sizes (3.1 Å and 1.55 Å, respectively). The initial microscope defocus and astigmatism parameters were determined with CTFFIND3 (27) and later refined with FREALIGN (16). During the initial stages of refinement, only the orientational parameters (translation center and three Euler angles) were refined. In later rounds of refinement, the absolute magnification was also refined on a per-particle image basis. The cryo-EM structure of Ad35f (38) filtered to 12-Å resolution was used as the starting model for refinement. A modified version of FREALIGN was used to allow the input of externally determined particle centers (38). After each round of refinement, several reconstructions were calculated with various thresholds for the "phase residual" parameter calculated by FREALIGN, which is a weighted correlation coefficient between particle and reference (16). The reconstruction with the highest resolution for the icosahedral capsid (radii of 300 to 463 Å) as assessed by the Fourier shell correlation (FSC) 0.5 threshold was selected as the input map for the subsequent round of refinement. After the final round of refinement, two types of Ad2*ts*1 density maps were calculated: one including only the capsid radial shell (300 to 463 Å) for resolution assessment and the other including all radial shells so that the reconstruction would include the core and fibers.

The final reconstruction presented in the figures includes 890 particle images, corresponding to 16% of the data. Additional reconstructions were also calculated with up to 4,229 particles, or 76% of the data. The reconstructions based on larger data subsets are nearly identical to the highest-resolution reconstruction based on 16% of the data, except that they have slightly worse resolutions. The map based on 76% of the data has an estimated resolution of 11.7 Å at the FSC 0.5 threshold, while the map based on 16% of the data has a resolution of 10.5 Å at the FSC 0.5 threshold.

In an attempt to examine the core structure, "core-only" reconstructions of Ad2*ts*1 and Ad35f were calculated with FREALIGN by setting the outer radius of the map to 300 Å or 325 Å. We applied various low-pass filters with resolution cutoffs in the range of 20 to 100 Å to the core-only maps and examined them with Chimera. No prominent, reproducible features were observed in either the Ad2*ts*1 or Ad35f core reconstructions.

A temperature factor (B = -300 Å^2) was applied to the highest-resolution Ad2*ts*1 and Ad35f reconstructions to restore high-resolution contrast using the BFACTOR program (http://emlab.rose2.brandeis.edu/grigorieff). The FSC and radial density plots were generated with MatLab.

Difference map analysis. A pseudoatomic facet composed of 18 copies of the Ad5 hexon trimer (Protein Data Bank no. 1P30) (36) and 3 copies of the Ad2 penton base pentamer with fiber peptide (Protein Data Bank no. 1X9T) (52) was generated. Optimal docked positions for hexon and penton base were found with the "Fit Model in Map" function of USCF Chimera (32). The pseudoatomic facet was filtered to the same resolution as the Ad2*ts*1 or control Ad35f (38) cryo-EM structure and subtracted from the cryo-EM density map with IMAGIC (45) to reveal density for the minor capsid proteins. All graphics figures were produced with USCF Chimera.

Mass calculations for the Ad2*ts*1 and Ad35f cores. The following assumptions were made for the mass calculations of the Ad2*ts*1 and Ad5 cores. Monomer copy numbers per virion were as follows: protein II (hexon), 720; protein III (penton base), 60; protein IIIa, 60; protein IV (fiber), 36; protein V, 170; protein VI, 369; protein VII, 633; protein VIII, 120; protein IX, 240; protein X (mu), 125; TP, 2; and protease, 43 for mature Ad and 9 for Ad2*ts*1. The copy number estimates for proteins V, VI, and VII are derived from mass spectrometry (20). Biochemical estimates are used for protein X (mu) (19) and TP (5, 34). The protease copy number of 43 in mature Ad is an average of three estimates, i.e., 10, 50, or 70 copies per virion (2, 4, 22), and the protease copy number in Ad2*ts*1 is reduced fivefold (2). Since the copy number of L1-52K in the mature Ad virion is controversial (7, 18) and since the copy number in the Ad2*ts*1 virion has been estimated as just one to two molecules (18), we left this protein out of the mass calculations. We assumed a mass of 23.7 MDa for the 36-kb dsDNA Ad2 and Ad5 genomes. Our calculations indicate that the mass of the Ad2*ts*1 core is ~46 MDa, versus ~44 MDa for mature Ad5 core (a 5% difference). When the internal capsid proteins are included in the calculation, the mass of the Ad2*ts*1 core is ~63 MDa, versus ~59 MDa for mature Ad5 (a 7% difference).

Quantification of core-plus-capsid and capsid-only average intensities in cryo-EM particle images. Subsets of 100 cryo-EM particle images included in the highest-resolution Ad2*ts*1 and Ad35f reconstructions were selected for analysis of their two-dimensional projection density. A third subset of 100 Ad2*ts*1 particle images that was excluded from the highest-resolution reconstruction but included in the reconstruction based on 76% of the data was also evaluated.

IMAGIC (45) was used to translationally center the selected particle images according to the refined FREALIGN centers (x,y). The centered particles were normalized (with the IMAGIC Norm-Variance command) and inverted (with the IMAGIC Arithmetic-with-Image command, Invert subcommand) so that protein density would have positive intensity values. Pixels with negative intensity values then were set to zero (with the IMAGIC Arithmetic-with-Image command, Threshold subcommand). A circular mask (radius = 300 Å) was applied to generate core-plus-capsid images, and radial masks (inner radius = 300 Å, outer radius = 463 Å) were applied to generate capsid-only images (with the IMAGIC Arithmetic-with-Image command, Circle and Ring subcommands). The core-plus-capsid images contain projection information from the core as well as from the top and bottom capsid surfaces. The capsid-only images contain projection information from only the capsid around the outer edge of the particle image (see Fig. S1 in the supplemental material). The IMAGIC Survey command was used to calculate the average intensities for the core-plus-capsid and capsid-only images.

Membrane disruption assay. Recombinant Ad5 protein VI and preprotein VI were expressed in BL21(DE3) cells and purified as previously described (50). Hexon protein was purified from Ad5-infected cells (41). Dioleoylphosphatidylcholine-dioleoylphosphatidylserine (75:25, mol%) liposomes containing 100 mM sulforhodamine B (SulfoB) were prepared as described previously (50). The effects of protein VI-hexon interactions on the in vitro membrane lytic activities of protein VI and preprotein VI were determined by first incubating protein VI or preprotein VI with increasing amounts of purified hexon for 30 min before addition to SulfoB-containing liposomes at 37°C. The extent of SulfoB released was measured 15 min after protein addition and expressed as a percentage of total SulfoB released upon treatment with 0.5% Triton X-100.

RESULTS

Cryo-EM structure reveals differences between the Ad2*ts*1 core and the mature Ad core. A 10.5-Å-resolution cryo-EM structure of the immature Ad2*ts*1 virion was calculated from 890 particle images selected from a total set of 5,544. Only a relatively low percentage (16%) of the Ad2*ts*1 particle images were included in the final, highest-resolution reconstruction. Additional reconstructions were calculated including 50 to 76% of the data; however, these had lower resolutions. This suggests either structural heterogeneity between the Ad2*ts*1 particles or variable signal-to-noise ratios in the cryoelectron micrographs. A comparison of selected particle images included in the 16% map versus those rejected from the 16% map but included in the 76% map indicates that there is variation in the signal-to-noise ratio. On average, the 76% map includes noisier particle images than are included in the highest-resolution, 16% map. We suspect that the long (~360-Å) and flexible Ad2 fiber present on the Ad2*ts*1 virions may lead to varying thicknesses of vitreous ice on the cryo-EM grids. This would in turn lead to variation in the signal-to-noise ratios in the micrographs.

The highest-resolution Ad2*ts*1 cryo-EM structure has an estimated resolution of 10.5 Å at the FSC 0.5 threshold (Fig. 1) (35). A cryo-EM structure of the mature Ad35f virion at 6.9-Å resolution (FSC 0.5) is shown for comparison (38). The Ad35f vector has an Ad5 capsid pseudotyped with an Ad35 fiber, which is relatively short (~130 Å). Except for the different fibers, the Ad35f cryo-EM structure serves as a reasonable comparison structure for Ad2*ts*1. Excluding fiber, the Ad2 and Ad5 structural proteins have identities of 86 to 100%. Therefore, the major differences between Ad2*ts*1 and Ad35f are the fibers (Ad2 versus Ad35), the variable hexon surface loops, and the presence of preproteins in Ad2*ts*1.

When both the Ad2*ts*1 and Ad35f cryo-EM structures are filtered to the same resolution (10.5 Å), their outer icosahedral capsid structures appear to be essentially indistinguishable, but

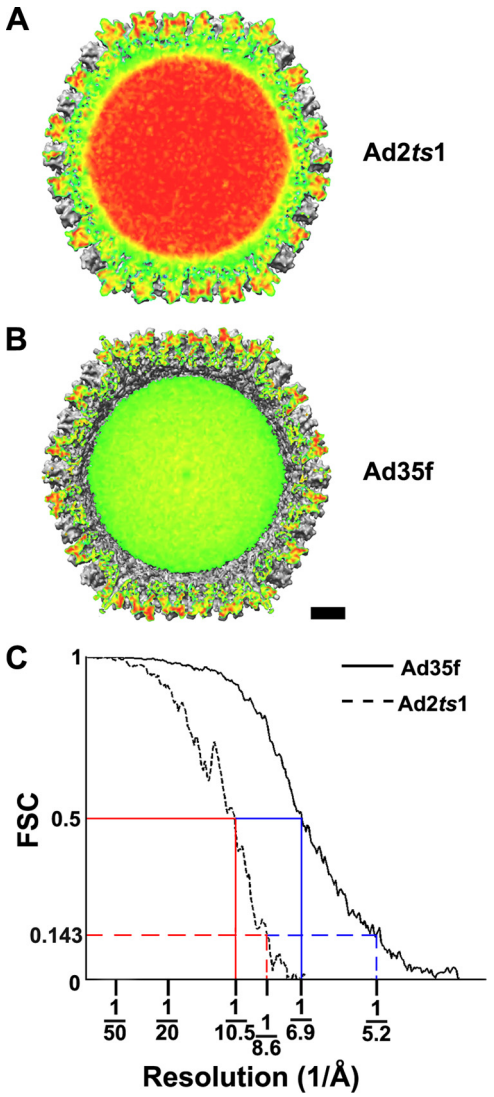

FIG. 1. Cryo-EM reconstructions of Ad2*ts*1 and Ad35f reveal a major structural difference in the core of the virion. (A) Cropped view of the Ad2*ts*1 reconstruction. The crop plane is colored by the density value, with the strongest density in red and the weakest in green. The protein/DNA-containing core displays predominantly strong density (red). (B) Cropped view of the Ad35f reconstruction (38) with the crop plane colored as in panel A. Both reconstructions are shown filtered to 10.5-Å resolution. Scale bar, 100 Å. (C) An FSC plot indicating a resolution range for Ad2*ts*1 of 10.5 Å to 8.6 Å (10.5 Å at FSC 0.5, 9.5 Å at FSC 0.3, and 8.6 Å at FSC 0.143). The resolution range for Ad35f is 6.9 Å to 5.2 Å (6.9 Å at FSC 0.5, 6.1 Å at FSC 0.3, and 5.2 Å at FSC 0.143).

the core regions differ considerably (Fig. 1 and 2). When the structures are colored by their reconstructed density values, as in Fig. 1, the Ad35f core (green to yellow) appears weaker than the surrounding capsid (green to red, with red representing the strongest reconstructed density values). In contrast, the Ad2*ts*1 core (red) appears stronger than its surrounding capsid (green to red). When the two structures are normalized to have the same means and standard deviations, the average reconstructed density value in the Ad2*ts*1 core is 44% greater than that in the Ad35f core. This effect is also evident in the average

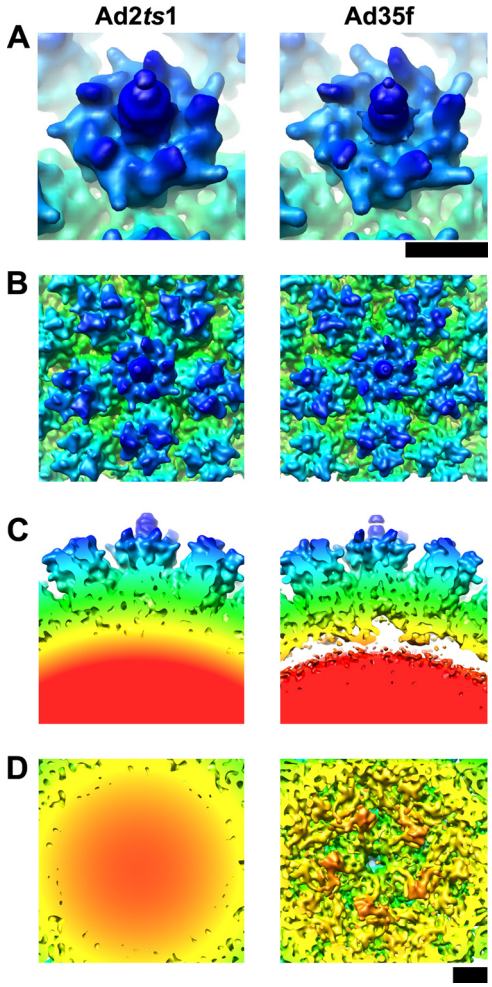

FIG. 2. The main differences between Ad2*ts*1 and Ad35f are on the interior of the icosahedral capsid. (A) Views of the penton base with a segment of protruding fiber. The fiber shafts of both virions are flexible, and thus only short portions are reconstructed. Both structures are shown filtered to 10.5-Å resolution and radially color coded (300 Å = red; 480 Å = blue). (B) Outer views of the vertex regions showing a penton base with five surrounding hexons. (C) Side views of the two vertex regions at similar isosurface contour levels. The Ad2*ts*1 capsid (yellow to blue) is closely associated with and connects to the core of the virion (red). In contrast, the Ad35f capsid is separated from the core by a gap in the density. (D) Inner views of the vertex regions showing the strong core density for Ad2*ts*1 and the resolved internal capsid density below the penton base and surrounding hexons for Ad35f. Scale bars, 50 Å.

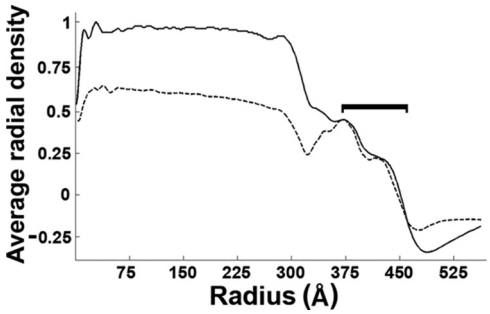

FIG. 3. Average radial density distributions of the Ad2*ts*1 and Ad35f structures. Profiles for Ad2*ts*1 (solid line) and Ad35f (dashed line) were calculated with the IMAGIC-5 Threed-radial-density-options routine. The two profiles were normalized in the radial shell (370 to 463 Å) indicated by the bracket and corresponding to the outer portion of the icosahedral capsid.

radial density profiles of the Ad2*ts*1 and Ad35f structures (Fig. 3). When the two profiles are normalized on the icosahedral capsids, the Ad2*ts*1 core has significantly stronger reconstructed density values. These findings indicate that either the immature core of Ad2*ts*1 is more ordered than the mature core of Ad35f or there is significantly more molecular mass within the Ad2*ts*1 core.

The proteome of the mature Ad5 virion has been analyzed in detail by mass spectrometry (7, 20, 21). Numerous biochemical and polyacrylamide gel electrophoresis analyses (17, 18, 29, 30) have indicated that the protein composition of Ad2*ts*1 is similar to that of the mature virion but with precursor forms of multiple viral proteins and a ~5-fold reduction in the encapsidation of protease. We estimated the total molecular masses of the Ad2*ts*1 and Ad35f cores by considering the copy numbers and molecular masses of the core components in both their immature forms (for Ad2*ts*1) and mature forms (for Ad35f). We also assumed that all of the small cleavage products generated by the Ad protease would be released from the virion. These calculations indicate a difference of 5 to 7% in total molecular mass between the Ad2*ts*1 and Ad5 cores, depending on whether or not the inner capsid proteins (IIIa, VI, and VIII) are included in the calculation. Although the mature core may have a slightly smaller total molecular mass than the immature core of Ad2*ts*1, our calculations indicate that the mass difference is not great enough to explain the significantly stronger reconstructed density values of the Ad2*ts*1 core.

The results of the molecular mass calculations for the Ad2*ts*1 and Ad35f cores are supported by an analysis of the cryo-EM particle images of Ad2*ts*1 and Ad35f. Using a subset of particle images included in either the highest-resolution Ad2*ts*1 reconstruction or the Ad35f reconstruction, we quantitated the average signal intensity from the core plus capsid within a radius of 300 Å and the average intensity from the capsid only within the radial shell of 300 to 463 Å (see Fig. S1 in the supplemental material). The ratio of the core-plus-capsid average intensity to the capsid-only average intensity in the two-dimensional projection images is essentially the same for Ad2*ts*1 and Ad35f, indicating that the Ad2*ts*1 core has approximately the same total molecular mass as the mature Ad core. Our working hypothesis for the observed core difference in the two reconstructions is that the Ad2*ts*1 has an increased level of icosahedral order.

The cryo-EM reconstruction also shows that the Ad2*ts*1 core extends to and appears to be connected to the capsid (Fig. 2C). Cryo-EM reconstructions of mature Ad virions, in contrast, show the core to be clearly separated from the capsid with a prominent gap below the capsid. These observations indicate that the Ad core condenses, or undergoes a structural rearrangement, during the maturation process. This is supported by a study showing that the Ad2*ts*1 chromatin is more resistant to micrococcal nuclease digestion than the mature Ad chromatin (29). Since the Ad2*ts*1 core appears to be connected to the capsid, condensation of the genome may be inhibited. The

immature core might possess a greater degree of icosahedral order by virtue of its association with the capsid, and this could lead to a more densely reconstructed core even without a significant difference in total mass.

The Ad2*ts*1 penton base is anchored to the viral core. One of the reported phenotypes of Ad2*ts*1 is its failure to release the fibers during cell entry (14), while wild-type Ad virions are thought to lose their fibers or vertices early in the cell entry pathway (15). This phenotype is somewhat difficult to explain because neither the penton base nor the fiber is cleaved by the viral protease, and thus Ad2*ts*1 contains the same forms of these proteins as in Ad2. Comparison of the vertex regions of the Ad2*ts*1 and Ad35f cryo-EM structures reveals no obvious difference between the outer proteins of the virion that could explain this property (Fig. 2A and B). The crystal structure of the Ad2 penton base with the N-terminal region of fiber (52) can be fit equally well into the vertex regions of the Ad2*ts*1 and Ad35f cryo-EM reconstructions. When the vertex region is viewed from inside the virion, well-resolved density below the penton base of Ad35f is observed, while only the dense core of Ad2*ts*1 can be seen (Fig. 2D). The density below the penton base includes protein IIIa (38, 39), which is presumably interacting with the N-terminal tails of penton base (amino acids [aa] 1 to 51) missing from the crystal structure.

Preprotein IIIa is cleaved by the protease, with the C-terminal 15 residues removed for both Ad2 and Ad5. The sequence of preprotein IIIa from these two serotypes indicates that there are three Arg residues in the C-terminal peptide that are removed by the protease. We speculate that these positively charged Arg residues may interact with the viral dsDNA genome. The cryo-EM structure of Ad2*ts*1 indicates that penton base is anchored to the viral core, presumably via the precursor form of protein IIIa.

Density inside the Ad2*ts*1 hexon cavities is assigned as preprotein VI. In order to more fully compare the structures of the minor capsid components in Ad2*ts*1 and Ad35f, we docked the atomic resolution structures of hexon (36) and penton base with the N-terminal fiber peptide (52) into the cryo-EM density and generated difference maps for both virions. The Ad2*ts*1 difference map shows density on the external capsid surface corresponding to the fiber shaft, the RGD-containing loop of penton base, surface loops of hexon missing from the crystal structure, and protein IX (Fig. 4A). In addition, the difference map also reveals density inside the cavity of every hexon trimer in the shape of a "plug," and this plug density clearly connects to the viral core (Fig. 4B and C). Less prominent density within the Ad35f hexons has also been assigned to protein VI on the basis of both biochemical and molecular genetic information (38, 51). Preprotein VI is cleaved by the protease, removing 33 aa from the N terminus and 11 aa from the C terminus for both Ad2 and Ad5. We tentatively assign the plug density found inside the cavity of every hexon in Ad2*ts*1 as the precursor form of protein VI.

Assignments for preproteins IIIa and VIII on the inner capsid. On the exterior capsid surface, the Ad2*ts*1 difference map reveals density assigned to the N- and C-terminal domains of protein IX (Fig. 5A). The dense core of Ad2*ts*1 complicates the analysis of the internal capsid proteins; however, strong density is observed at the locations assigned to mature proteins IIIa and VIII in Ad35f (Fig. 5B). While the mature forms of

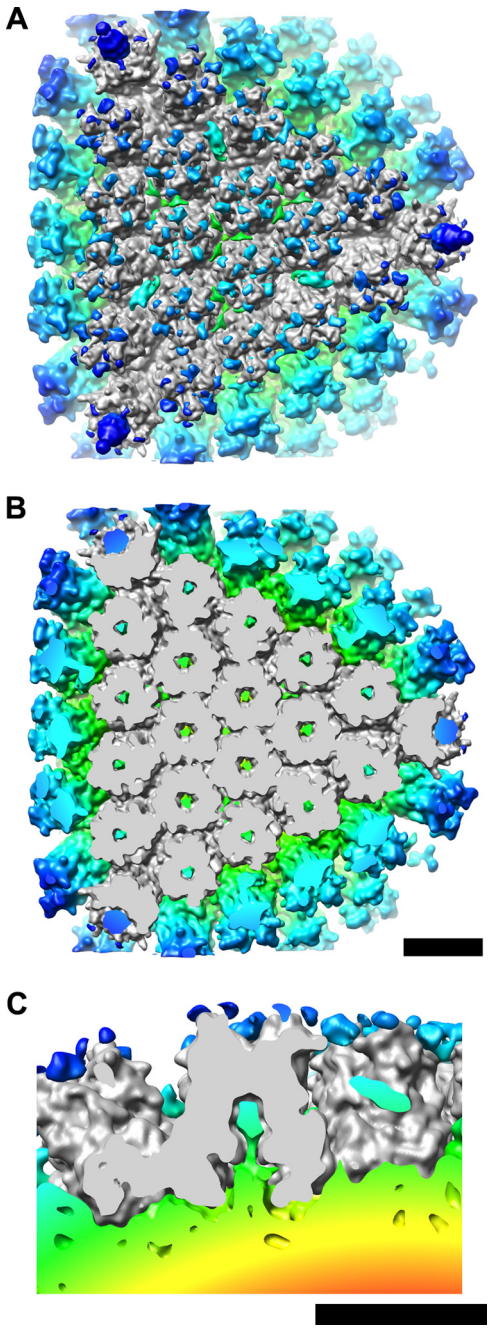

FIG. 4. Preprotein VI is assigned to density within the cavity of every hexon trimer in Ad2*ts*1. (A) An enlarged facet (gray) consisting of docked crystal structures of 18 hexon trimers and 3 penton base pentamers is shown filtered to 10.5-Å resolution. The facet is superimposed on the Ad2*ts*1 difference density, which is radially color coded as in Fig. 2. The external difference density includes the protruding fiber shaft, surface loops of hexon and penton base missing from their respective crystal structures, and density assigned to protein IX. (B) Cropping away the top ~80 Å of the facet reveals difference density inside of every hexon trimer (green). Similar density within the Ad35f hexons has been assigned to protein VI (38). The density within every hexon of Ad2*ts*1 is tentatively assigned as preprotein VI. (C) Side cropped view of a peripentonal hexon within the facet (gray) with the internal difference density in the shape of a "plug," which connects to the Ad2*ts*1 core (yellow to red). Scale bars, 100 Å.

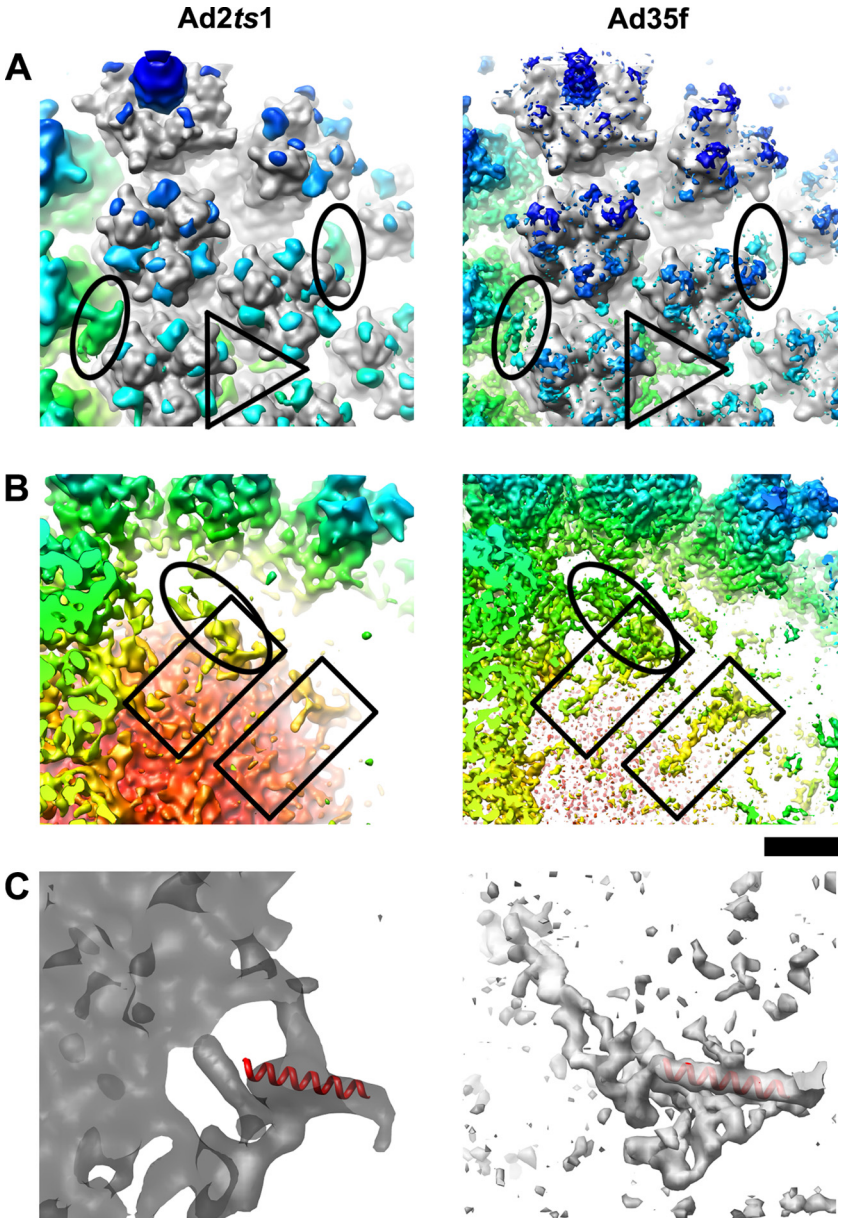

FIG. 5. Density assigned to protein IX and preproteins IIIa and VIII is found within Ad2*ts*1. (A) The Ad2*ts*1 difference map (filtered to 10.5 Å) and the Ad35f difference map (filtered to 10.5 Å resolution) are shown superimposed on a portion of the facet (gray). The density assigned to the N-terminal domain of protein IX is outlined with triangles, and that assigned to the C-terminal domain of protein IX is within ovals (38). (B) Cropping away the top ~100 Å reveals internal difference density below the penton base and hexons assigned to preproteins IIIa (oval) and VIII (rectangle) in Ad2*ts*1 and the mature forms of proteins IIIa and VIII in Ad35f. (C) Rotating by 180° and enlarging one copy of preprotein VIII (left, transparent) or mature protein VIII (right, transparent) shows the density rod assigned to the predicted 22-aa α-helix (red) in fragment 1 of protein VIII. In panel C the Ad35f density is shown filtered to 6.9 Å so that α-helical rod is well resolved. The internal Ad2*ts*1 difference density in panels B and C is shown with a relatively high isosurface contour level (0.65σ, versus 0.37σ in panel A) so that the density assigned to precursor proteins can be resolved from the core. The Ad35f difference density is shown with an isosurface contour level of 0.85σ to reveal the α-helical nature of the C-terminal domain of proteins IX, as well as proteins IIIa and VIII. In panels A and B the Ad2*ts*1 and Ad35f difference density maps are shown radially color coded as in Fig. 2. Scale bar, 50 Å.

proteins IIIa and VIII are separated from the core in Ad35f, the precursor forms in Ad2*ts*1 appear to be anchored to the core. Both preproteins IIIa and VIII are cleaved by the protease, which could lead to their separation from the core.

Mass spectrometry has indicated that the Ad5 preprotein VIII is cleaved at two sites, with the resulting fragment 1 (12.1 kDa) and fragment 3 (7.6 kDa) retained in the mature virion (20). It is not clear whether fragment 2 of protein VIII is retained or released. The resolution of the Ad35f cryo-EM structure, 6.9 Å, is high enough to reveal α-helices within protein IIIa and the density assigned to protein VIII (38). The observation of one relatively long (~35-Å) α-helix in the protein VIII density (Fig. 5C) is consistent with the secondary structure prediction of a ~22-aa α-helix in fragment 1 (see Fig.

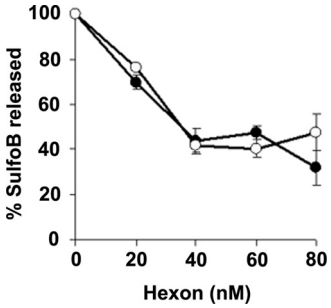

FIG. 6. Hexon binding shields protein VI and preprotein VI membrane lytic activities. Recombinant protein VI or preprotein VI was incubated with increasing amounts of purified hexon for 30 min before addition to SulfoB-containing liposomes at 37°C. The percentage of SulfoB released was measured 15 min after protein addition to liposomes. Protein VI (black circles) or preprotein VI (white circles) was present at a final concentration of 20 nM. Error bars represent standard errors of the means.

S2 in the supplemental material). The more moderate resolution of the Ad2*ts*1 cryo-EM structure, 10.5 Å, does not show as clearly resolved α-helices. Nevertheless, Ad2*ts*1 does appear to contain a density rod at the same site, suggesting that the N-terminal region of preprotein VIII (aa 1 to 111) is associated with the capsid.

Hexon shields protein VI and preprotein VI membrane lytic activity. Protein VI has long been referred to as a hexon-associated protein (8, 25). More recently, protein VI has been identified as a membrane lytic factor of Ad (50). Both recombinant protein VI and its precursor form have been shown to possess membrane lytic activity in liposome disruption assays. Here we present data showing that purified hexon inhibits the membrane lytic activities of both protein VI and preprotein VI (Fig. 6). Inhibition was saturable, with a maximal reduction in membrane lytic activity of ~60%. These results indicate that the membrane lytic domains of protein VI and preprotein VI are equivalently shielded by hexon.

DISCUSSION

The Ad core condenses and becomes less symmetrically ordered during maturation. The Ad2*ts*1 cryo-EM structure indicates that the core of this mutant virus is connected to the icosahedral capsid and that the core may have partial icosahedral order. As the wild-type Ad core undergoes maturation, involving the proteolytic cleavage of precursors of seven core and inner capsid proteins, the core condenses and separates from the icosahedral outer capsid, leading to a less symmetrically arranged structure for the DNA/protein viral core. The moderate resolution (~10 Å) of the Ad2*ts*1 cryo-EM structure does not allow us to visualize precisely which precursor proteins are mediating the capsid/core association in Ad2*ts*1. However, two studies have found that the capsid protein VI interacts with the core protein V (6, 24). Therefore, we deduce that the preprotein VI, which is present in ~369 copies per virion (20), is likely to bind to both hexon in the capsid and protein V in the core and contribute to the observed capsid/core connection in Ad2*ts*1. This is in agreement with observations by Mirza and Weber that preprotein VI is associated with Ad2*ts*1 cores isolated by pyridine treatment but that protein VI is not associated with mature cores (29, 30). Preprotein IIIa, which is present in 60 copies per virion and which is underneath the vertices, is also likely to contribute to the observed Ad2*ts*1 capsid/core connection. The protein IIIa precursor may be anchored to the Ad2*ts*1 core by its arginine-rich C-terminal peptide region. The protease removes the arginine-rich region, and thus the mature protein IIIa may be more closely associated with the capsid than with the core.

Vertex release may require a conformational change that is blocked in Ad2*ts*1. A conformational change in the vertex region has been proposed after the interaction of Ad with integrins on the cell surface (14). Alternatively, conformational changes in the vertex proteins may be triggered by the low-pH environment of the endosome. These conformational changes are thought to lead to release of the vertex proteins, including penton base, fiber, protein IIIa, and the membrane lytic protein VI (50). Comparison of the Ad2*ts*1 cryo-EM structure with that of Ad35f, which contains the mature Ad5 structural proteins with an Ad35 fiber, indicates no obvious differences on the outer surface of the icosahedral capsid. Differences are found, however, on the inner surface of the capsid below the penton base. Docking of the crystal structure into cryo-EM Ad structures shows that the N-terminal 51-aa tails of penton base, which are missing from the crystal structure, are oriented toward the viral core (9, 37, 38). We have previously postulated that the N-terminal tails of penton base interact with protein IIIa in the mature Ad virion (38). It seems likely that this interaction also occurs in Ad2*ts*1 with preprotein IIIa. Anchoring of the penton base to the Ad2*ts*1 core via the preprotein IIIa may block the proposed conformational change in the vertex region (Fig. 7). Additionally, anchoring of the hexons to the immature core by preprotein VI may also contribute to the higher stability of Ad2*ts*1.

The stability of Ad2*ts*1 can be partially overcome by high temperature. In vitro uncoating assays with Ad2*ts*1 indicate that ~50% of penton base, fiber, and protein IIIa is released at pH 7.4 and 50°C, while ~100% of preprotein VI is retained in the virion (50). In contrast, wild-type Ad5 virions at the same pH release the vertex proteins (penton base, fiber, and protein IIIa) together with protein VI and at a lower temperature of ~45°C. Another study comparing the uncoating of Ad2*ts*1 and Ad5 found that for Ad5 at neutral pH, protein VI and fiber both dissociated at 49°C. For Ad2*ts*1, fiber dissociation occurred at 49°C, but preprotein VI dissociation was observed only at above 67°C (42). This uncoating information together with the Ad2*ts*1 structure indicates that vertex release is inhibited in Ad2*ts*1 and that even if this inhibition is overcome with high temperature (50 to 67°C), preprotein VI remains firmly anchored to the immature core.

It has been shown previously that both protein VI and preprotein VI have membrane lytic activity (50). We present data indicating that hexon can shield the membrane lytic activities of both the mature and preprotein forms of protein VI equally well. Thermal disassembly studies indicate that mature wild-type Ad virions release ~80% of penton base with ~25% of the hexons in the Ad capsid and a large percentage (~80%) of protein VI (50). If the cryo-EM density assignment for protein VI is correct and protein VI is associated with all of the hexons in the capsid, then homo-

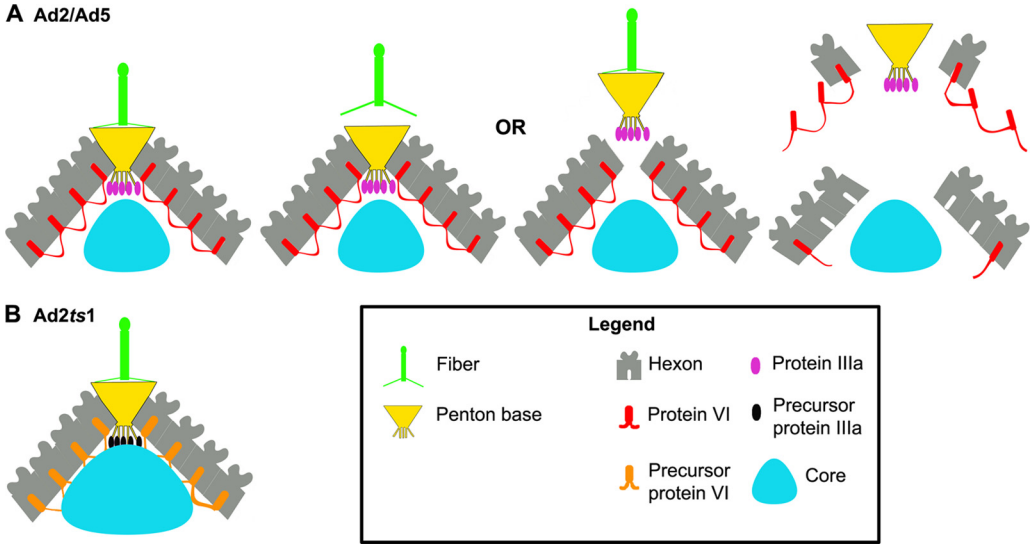

FIG. 7. Diagram of proposed cell entry events for Ad2 and Ad5 versus Ad2*ts*1. (A) One vertex of an Ad2 or Ad5 virion is shown schematically (left). The location of protein IIIa (magenta ovals) underneath the penton base is as assigned by a cryo-EM study (38) and confirmed by a peptide tagging study (39). The position of protein VI (red) within the cavity of every hexon trimer is as assigned by cryo-EM (38). We propose that a critical step of disassembly is either release of the fiber or release of the fiber/penton base complex (middle). Vertex release is associated with release of 25% of the hexons and 80% of protein VI (right), as shown by Wiethoff et al. (50) for Ad5 at temperatures over 45°C. (B) One vertex of an Ad2*ts*1 virion is shown schematically, with preprotein IIIa (black ovals) and preprotein VI (orange) anchored to the immature DNA/protein core (cyan). The association of preprotein IIIa with both the N-terminal tails of penton base and the viral core may impede the release of the vertex proteins (fiber, penton base, and preprotein IIIa). In addition, anchoring of preprotein VI to the core may block its release.

typic interactions between protein VI monomers would explain the simultaneous release of a high percentage of this protein (Fig. 7A) (38). Uncoating assays indicate that the preprotein VI is not released from Ad2*ts*1 even at 60°C (pH 7.4). The cryo-EM structure indicates that preprotein VI is associated with both the capsid hexons and the immature core (Fig. 7B), and presumably the interaction with the core is stronger. Since preprotein VI is not released, Ad2*ts*1 cannot escape from the endosome in a timely manner and is targeted to lysosomes for degradation (14).

In conclusion, the cryo-EM structure of Ad2*ts*1 reveals a virion in which the core protein/DNA has not condensed and separated from the capsid as in mature Ad. The interaction between the capsid and core is presumably mediated by one or more of the precursor proteins, with IIIa and VI being likely candidates. Preprotein IIIa has an arginine-rich C-terminal peptide tail, which is cleaved by the protease and which may associate with the dsDNA viral genome. Protein VI is known to associate with core protein V (6, 24), and preprotein VI is retained in pyridine cores (30), making it a second likely candidate. The cryo-EM observation that the Ad2*ts*1 capsid and core are associated is consistent with functional studies showing that Ad2*ts*1 is more stable than wild-type mature virions (17, 50). The finding that Ad2*ts*1 fails to release its vertex proteins (14), combined with the cryo-EM observation of no obvious differences between the external surfaces of Ad2*ts*1 and a mature Ad virion, indicates that the capsid/core connection plays a role in the disassembly defect of Ad2*ts*1. Our structural analyses suggest that vertex release and disassembly are impeded in Ad2*ts*1 by linkage of the penton base to preprotein IIIa and to the immature core.

ACKNOWLEDGMENTS

Sources of funding for this work include NIH grant AI42929 (P.L.S.), NIH grant EY011431 (G.R.N.), NIH grant HL054352 (G.R.N.), and IDPH grant 86280165 (C.M.W.). M.S. acknowledges support from an NIH molecular biophysics training grant at Vanderbilt (T32-GM008320), and J.G.S. acknowledges support from NIAID grant F32-AI072936.

We gratefully acknowledge computer support from the Advanced Computing Center for Research & Education (ACCRE) at Vanderbilt.

REFERENCES

1. **Adiga, U., W. T. Baxter, R. J. Hall, B. Rockel, B. K. Rath, J. Frank, and R. Glaeser.** 2005. Particle picking by segmentation: a comparative study with SPIDER-based manual particle picking. J. Struct. Biol. **152:**211–220.
2. **Anderson, C. W.** 1990. The proteinase polypeptide of adenovirus serotype 2 virions. Virology **177:**259–272.
3. **Bergelson, J. M., J. A. Cunningham, G. Droguett, E. A. Kurt-Jones, A. Krithivas, J. S. Hong, M. S. Horwitz, R. L. Crowell, and R. W. Finberg.** 1997. Isolation of a common receptor for coxsackie B viruses and adenoviruses 2 and 5. Science **275:**1320–1323.
4. **Brown, M. T., W. J. McGrath, D. L. Toledo, and W. F. Mangel.** 1996. Different modes of inhibition of human adenovirus proteinase, probably a cysteine proteinase, by bovine pancreatic trypsin inhibitor. FEBS Lett. **388:** 233–237.
5. **Challberg, M. D., S. V. Desiderio, and T. J. Kelly, Jr.** 1980. Adenovirus DNA replication in vitro: characterization of a protein covalently linked to nascent DNA strands. Proc. Natl. Acad. Sci. USA **77:**5105–5109.
6. **Chatterjee, P. K., M. E. Vayda, and S. J. Flint.** 1985. Interactions among the three adenovirus core proteins. J. Virol. **55:**379–386.
7. **Chelius, D., A. F. Huhmer, C. H. Shieh, E. Lehmberg, J. A. Traina, T. K. Slattery, and E. Pungor, Jr.** 2002. Analysis of the adenovirus type 5 proteome by liquid chromatography and tandem mass spectrometry methods. J. Proteome Res. **1:**501–513.
8. **Everitt, E., L. Lutter, and L. Philipson.** 1975. Structural proteins of adenoviruses. XII. Location and neighbor relationship among proteins of adenovirion type 2 as revealed by enzymatic iodination, immunoprecipitation and chemical cross-linking. Virology **67:**197–208.
9. **Fabry, C. M., M. Rosa-Calatrava, J. F. Conway, C. Zubieta, S. Cusack, R. W.**

Ruigrok, and G. Schoehn. 2005. A quasi-atomic model of human adenovirus type 5 capsid. EMBO J. **24:**1645–1654.
10. **Fabry, C. M., M. Rosa-Calatrava, C. Moriscot, R. W. Ruigrok, P. Boulanger, and G. Schoehn.** 2009. The C-terminal domains of adenovirus serotype 5 protein IX assemble into an antiparallel structure on the facets of the capsid. J. Virol. **83:**1135–1139.
11. **Furcinitti, P. S., J. van Oostrum, and R. M. Burnett.** 1989. Adenovirus polypeptide IX revealed as capsid cement by difference images from electron microscopy and crystallography. EMBO J. **8:**3563–3570.
12. **Gaggar, A., D. M. Shayakhmetov, and A. Lieber.** 2003. CD46 is a cellular receptor for group B adenoviruses. Nat. Med. **9:**1408–1412.
13. **Gastaldelli, M., N. Imelli, K. Boucke, B. Amstutz, O. Meier, and U. F. Greber.** 2008. Infectious adenovirus type 2 transport through early but not late endosomes. Traffic **9:**2265–2278.
14. **Greber, U. F., P. Webster, J. Weber, and A. Helenius.** 1996. The role of the adenovirus protease on virus entry into cells. EMBO J. **15:**1766–1777.
15. **Greber, U. F., M. Willetts, P. Webster, and A. Helenius.** 1993. Stepwise dismantling of adenovirus 2 during entry into cells. Cell **75:**477–486.
16. **Grigorieff, N.** 2007. FREALIGN: high-resolution refinement of single particle structures. J. Struct. Biol. **157:**117–125.
17. **Hannan, C., L. H. Raptis, C. V. Dery, and J. Weber.** 1983. Biological and structural studies with an adenovirus type 2 temperature-sensitive mutant defective for uncoating. Intervirology **19:**213–223.
18. **Hasson, T. B., D. A. Ornelles, and T. Shenk.** 1992. Adenovirus L1 52- and 55-kilodalton proteins are present within assembling virions and colocalize with nuclear structures distinct from replication centers. J. Virol. **66:**6133–6142.
19. **Hosokawa, K., and M. T. Sung.** 1976. Isolation and characterization of an extremely basic protein from adenovirus type 5. J. Virol. **17:**924–934.
20. **Lehmberg, E., J. A. Traina, J. A. Chakel, R. J. Chang, M. Parkman, M. T. McCaman, P. K. Murakami, V. Lahidji, J. W. Nelson, W. S. Hancock, E. Nestaas, and E. Pungor, Jr.** 1999. Reversed-phase high-performance liquid chromatographic assay for the adenovirus type 5 proteome. J. Chromatogr. B **732:**411–423.
21. **Liu, Y.-H., G. Vellekamp, G. Chen, U. A. Mirza, D. Wylie, B. Twarowska, J. T. Tang, F. W. Porter, S. Wang, T. L. Nagabhushan, and B. N. Pramanik.** 2003. Proteomic study of recombinant adenovirus 5 encoding human p53 by matrix-assisted laser desorption/ionization mass spectrometry in combination with database search. Int. J. Mass Spectrom. **226:**55–69.
22. **Mangel, W. F., M. L. Baniecki, and W. J. McGrath.** 2003. Specific interactions of the adenovirus proteinase with the viral DNA, an 11-amino-acid viral peptide, and the cellular protein actin. Cell. Mol. Life Sci. **60:**2347–2355.
23. **Marsh, M. P., S. K. Campos, M. L. Baker, C. Y. Chen, W. Chiu, and M. A. Barry.** 2006. Cryoelectron microscopy of protein IX-modified adenoviruses suggests a new position for the C terminus of protein IX. J. Virol. **80:**11881–11886.
24. **Matthews, D. A., and W. C. Russell.** 1998. Adenovirus core protein V is delivered by the invading virus to the nucleus of the infected cell and later in infection is associated with nucleoli. J. Gen. Virol. **79:**1671–1675.
25. **Matthews, D. A., and W. C. Russell.** 1995. Adenovirus protein-protein interactions: molecular parameters governing the binding of protein VI to hexon and the activation of the adenovirus 23K protease. J. Gen. Virol. **76:**1959–1969.
26. **McGrath, W. J., A. P. Abola, D. L. Toledo, M. T. Brown, and W. F. Mangel.** 1996. Characterization of human adenovirus proteinase activity in disrupted virus particles. Virology **217:**131–138.
27. **Mindell, J. A., and N. Grigorieff.** 2003. Accurate determination of local defocus and specimen tilt in electron microscopy. J. Struct. Biol. **142:**334–347.
28. **Mirza, A., and J. Weber.** 1980. Infectivity and uncoating of adenovirus cores. Intervirology **13:**307–311.
29. **Mirza, M. A., and J. Weber.** 1982. Structure of adenovirus chromatin. Biochim. Biophys. Acta **696:**76–86.
30. **Mirza, M. A., and J. Weber.** 1979. Uncoating of adenovirus type 2. J. Virol. **30:**462–471.
31. **Nemerow, G. R., L. Pache, V. Reddy, and P. L. Stewart.** 2009. Insights into adenovirus host cell interactions from structural studies. Virology **384:**380–388.
32. **Pettersen, E. F., T. D. Goddard, C. C. Huang, G. S. Couch, D. M. Greenblatt, E. C. Meng, and T. E. Ferrin.** 2004. UCSF Chimera—a visualization system for exploratory research and analysis. J. Comput. Chem. **25:**1605–1612.
33. **Rancourt, C., H. Keyvani-Amineh, S. Sircar, P. Labrecque, and J. M. Weber.** 1995. Proline 137 is critical for adenovirus protease encapsidation and activation but not enzyme activity. Virology **209:**167–173.
34. **Rekosh, D. M., W. C. Russell, A. J. Bellet, and A. J. Robinson.** 1977. Identification of a protein linked to the ends of adenovirus DNA. Cell **11:**283–295.
35. **Rosenthal, P. B., and R. Henderson.** 2003. Optimal determination of particle orientation, absolute hand, and contrast loss in single-particle electron cryomicroscopy. J. Mol. Biol. **333:**721–745.
36. **Rux, J. J., P. R. Kuser, and R. M. Burnett.** 2003. Structural and phylogenetic analysis of adenovirus hexons by use of high-resolution X-ray crystallographic, molecular modeling, and sequence-based methods. J. Virol. **77:**9553–9566.
37. **Saban, S. D., R. R. Nepomuceno, L. D. Gritton, G. R. Nemerow, and P. L. Stewart.** 2005. CryoEM structure at 9A resolution of an adenovirus vector targeted to hematopoietic cells. J. Mol. Biol. **349:**526–537.
38. **Saban, S. D., M. Silvestry, G. R. Nemerow, and P. L. Stewart.** 2006. Visualization of alpha-helices in a 6-angstrom resolution cryoelectron microscopy structure of adenovirus allows refinement of capsid protein assignments. J. Virol. **80:**12049–12059.
39. **San Martin, C., J. N. Glasgow, A. Borovjagin, M. S. Beatty, E. A. Kashentseva, D. T. Curiel, R. Marabini, and I. P. Dmitriev.** 2008. Localization of the N-terminus of minor coat protein IIIa in the adenovirus capsid. J. Mol. Biol. **383:**923–934.
40. **Shi, J., D. R. Williams, and P. L. Stewart.** 2008. A script-assisted microscopy (SAM) package to improve data acquisition rates on FEI Tecnai electron microscopes equipped with Gatan CCD cameras. J. Struct. Biol. **164:**166–169.
41. **Smith, J. G., A. Cassany, L. Gerace, R. Ralston, and G. R. Nemerow.** 2008. Neutralizing antibody blocks adenovirus infection by arresting microtubule-dependent cytoplasmic transport. J. Virol. **82:**6492–6500.
42. **Smith, J. G., and G. R. Nemerow.** 2008. Mechanism of adenovirus neutralization by human alpha-defensins. Cell Host Microbe **3:**11–19.
43. **Stewart, P. L., R. M. Burnett, M. Cyrklaff, and S. D. Fuller.** 1991. Image reconstruction reveals the complex molecular organization of adenovirus. Cell **67:**145–154.
44. **Suomalainen, M., M. Y. Nakano, S. Keller, K. Boucke, R. P. Stidwill, and U. F. Greber.** 1999. Microtubule-dependent plus- and minus end-directed motilities are competing processes for nuclear targeting of adenovirus. J. Cell Biol. **144:**657–672.
45. **van Heel, M., G. Harauz, E. V. Orlova, R. Schmidt, and M. Schatz.** 1996. A new generation of the IMAGIC image processing system. J. Struct. Biol. **116:**17–24.
46. **Weber, J.** 1976. Genetic analysis of adenovirus type 2 III. Temperature sensitivity of processing viral proteins. J. Virol. **17:**462–471.
47. **Weber, J. M.** 1995. Adenovirus endopeptidase and its role in virus infection. Curr. Top. Microbiol. Immunol. **199:**227–235.
48. **Webster, A., S. Russell, P. Talbot, W. C. Russell, and G. D. Kemp.** 1989. Characterization of the adenovirus proteinase: substrate specificity. J. Gen. Virol. **70:**3225–3234.
49. **Wickham, T. J., P. Mathias, D. A. Cheresh, and G. R. Nemerow.** 1993. Integrins alpha v beta 3 and alpha v beta 5 promote adenovirus internalization but not virus attachment. Cell **73:**309–319.
50. **Wiethoff, C. M., H. Wodrich, L. Gerace, and G. R. Nemerow.** 2005. Adenovirus protein VI mediates membrane disruption following capsid disassembly. J. Virol. **79:**1992–2000.
51. **Wodrich, H., T. Guan, G. Cingolani, D. Von Seggern, G. Nemerow, and L. Gerace.** 2003. Switch from capsid protein import to adenovirus assembly by cleavage of nuclear transport signals. EMBO J. **22:**6245–6255.
52. **Zubieta, C., G. Schoehn, J. Chroboczek, and S. Cusack.** 2005. The structure of the human adenovirus 2 penton. Mol. Cell **17:**121–135.